

Article

# Assessment of the Seismic Vulnerability of Bridge Abutments with 3D Numerical Simulations

Davide Forcellini 

Faculty of Civil Engineering, University of San Marino, Via Consiglio dei Sessanta 99, 47890 Serravalle, San Marino; [davide.forcellini@unirsm.sm](mailto:davide.forcellini@unirsm.sm)

**Abstract:** The role of abutments on the seismic vulnerability of bridges has been relatively little studied in geotechnical literature. To cover this gap, 3D numerical simulations were herein performed, by studying the seismic performance of three single-span bridge configurations. The numerical models used OpenSees to account the effects due to soil structure interaction between the deck and the abutments. In particular, advanced materials were implemented to model the non-linear hysteresis and plasticity that are responsible for soil deformations and, thus, structural damage. A probabilistic-based approach was considered and analytical fragility curves were developed to account modeling uncertainties. The role of bridge deformability was investigated by considering several limit states based on the calculation of the longitudinal displacements of the deck.

**Keywords:** seismic vulnerability; abutments; analytical fragility curves; numerical simulations; OpenSees



**Citation:** Forcellini, D. Assessment of the Seismic Vulnerability of Bridge Abutments with 3D Numerical Simulations. *Geosciences* **2022**, *12*, 316. <https://doi.org/10.3390/geosciences12090316>

Academic Editors:  
Jesus Martinez-Frias and  
Antonio Formisano

Received: 6 June 2022

Accepted: 22 August 2022

Published: 25 August 2022

**Publisher's Note:** MDPI stays neutral with regard to jurisdictional claims in published maps and institutional affiliations.



**Copyright:** © 2022 by the author. Licensee MDPI, Basel, Switzerland. This article is an open access article distributed under the terms and conditions of the Creative Commons Attribution (CC BY) license (<https://creativecommons.org/licenses/by/4.0/>).

## 1. Background

Fragility curves may be considered a credited approach for assessing the seismic vulnerability of bridges, and consist of representing the relationship between the seismic hazard and the level of structural damage related to selected earthquake scenarios. In order to develop fragility curves, the selection of the intensity measure (IM) is a fundamental issue, as demonstrated by [1,2] that investigated different scalar IMs or couples of IMs to derive fragility curves as a function of alternative variables. Other researchers (i.e., [3,4]) studied the accuracy of several IMs, such as Fajfar index ( $I_v$ ), peak ground velocity (PGV), root mean square velocity (RMS), and spectral acceleration ( $S_a$ ), in terms of efficiency, proficiency and sufficiency. In addition, many contributions have proposed non-linear dynamic analyses for RC bridge seismic assessment (i.e., [5–8]) to derive structural demand evaluations at increasing IM levels. In this regard, the choice of IMs is fundamental in developing fragility curves, and many attempts have been proposed to investigate the most representative IM. However, (1) there are many uncertainties that depend on the structure or even on the demand parameters [9], and (2) many researchers have demonstrated that no IM can fully represent the effects of an earthquake on the seismic demand of structures (Li et al., 2014; [10]) because of the complexity of earthquake ground motions. In a structural arena, [11] proposed to apply the geometric mean of spectral acceleration in probabilistic seismic demand analysis (PSDA), finding that such IM may be applied as a predictor of structural response. In addition, [12] proposed to investigate the use of spectral acceleration averaged over a period range as an intensity measure (IM) for assessing the risk of collapse for nearly 700 moment-resisting frame and shear wall structures of various heights and different ground motion sets.

Hybrid solutions were also proposed, such as an average spectral acceleration based on the  $S_a$  values [13], multiple IMs [1], a vector-valued intensity measure VIM [14,15], and a fractional order IM by [3]. However, the most commonly used IMs in the bridge arena are peak ground acceleration (PGA, i.e., [3]) and Spectral Acceleration (SA) at the fundamental

period [16–19]. In addition, even if fragility curves were also proposed in literature for bridge classes, most of these contributions have investigated multi-span bridges, rather than concentrating on single infrastructure network components.

The principal motivation of this paper is to fill this gap by focusing on single-span bridges by exploring the role of abutments on the seismic vulnerability of the entire structural performance. In addition, this paper aims to investigate abutment–embankment stiffness, which is one of the most important issues in the assessment of bridge abutments. In this regard, Caltrans is probably the most credited quantitative guidance currently available worldwide, being based on several full-scale tests at the University of California: at UC Davis [20], San Diego [21] and Los Angeles (UCLA, [22]). In this context, this paper is organized in the following steps: (1) the assessment of different IMs to represent the seismic hazard, (2) the development of fragility functions for single span bridges, and, (3) a case study to assess the accuracy of different IMs when predicting damage at the abutments.

## 2. Case Study

This section shows the design of the selected bridge configurations that were selected in order to focus on the role of abutments on the seismic vulnerability of the structure. In this regard, the configurations consist of single-span bridge with several geometric characteristics.

### 2.1. Bridge Model

This paper aims to consider three configurations of single-span bridge configurations that represent typical Californian bridges. Three-dimensional finite element analysis was employed to consider the effects of the rotations along the vertical and transversal axes, which is not possible to simulate in two-dimensional finite element analysis. Thus, state-of-the-art open access software OpenSees [23] was employed. The developed finite element model is shown in Figure 1 (3D and schematic plan view) and was built following previous numerical models [24–26]. Since the designed longitudinal elastomeric bearing pads on the abutments perform correctly, the deck may be assumed to be capacity designed so that it is able to respond in the elastic range. The decks were modelled using beam elements with linear elastic properties. The cross section (A), the moments of inertial in the transversal and longitudinal directions (ITR, ILG), are shown in Table 1. A linear elastic model was employed to model the concrete deck: the modulus of elasticity of the concrete, Poisson's ratio and the unit weight were considered equal to  $2.8 \times 10^4$  MPa, 0.20, and 24 kN/m<sup>3</sup>, respectively. The deck slabs were connected with the abutments with elastomeric bearing pads, whose characteristics are shown in Table 2.

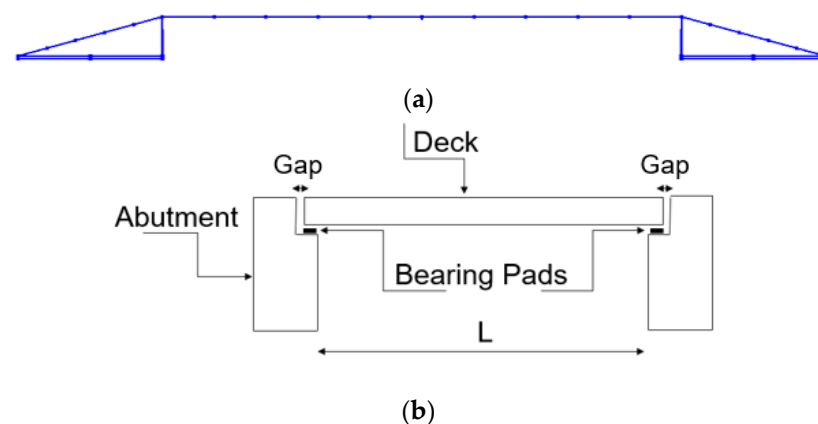


Figure 1. (a) 3D finite element models; (b) plan view of the bridge.

**Table 1.** Geometric and material properties of decks.

	L (ft)	L (m)	A (m <sup>2</sup> )	I <sub>TR</sub> (m <sup>4</sup> )	I <sub>LG</sub> (m <sup>4</sup> )
B1	40	12.19	3.36	1.65	31.71
B2	60	18.29	3.46	1.70	32.56
B3	80	24.38	3.61	1.77	33.97

**Table 2.** Geometric and material properties of bearing pads.

Bearing Pads: Properties	Values
Number	3
Height (m)	0.05
Shear modulus G (kPa)	1034
Young modulus E (kPa)	34,474
Yield displacement (%)	150
Ultimate displacement (%)	300

## 2.2. Abutment Model

This section shows the design of the selected bridge configurations selected in order to focus on the role of abutments on the seismic vulnerability of the structure. In this regard, the configurations consist of a single-span bridge with several geometric characteristics. Abutments are built to provide an economical means of resisting bridge inertial seismic loads. As demonstrated by [27], the traditional theories based on active and passive earth pressures cannot be used during seismic events since the massive bridge structure induces higher than anticipated passive earth pressure conditions. This is mainly true for Ordinary Standard bridge structures in California with short spans and relatively high superstructure stiffness, where the embankment mobilization and inelastic behaviour of the soil material under high shear deformation levels dominate the response of the whole bridge [28,29]. In particular, the abutment participating mass has a critical effect on the mode shapes and consequently the dynamic response of the bridge, as shown in [29]. In addition, the role of soil structure interaction is fundamental to account for the non-linear behaviours that may occur. In this regard, short-span bridges are the most affected by the resistance-induced mechanisms and mass of the abutment.

In order to realistically model those bridges, [29] suggested using the spring model, since the simplified abutment model may considerably underestimate the transversal displacements and, thus, underestimate the risk of shear key failures. In the present paper, the spring model was applied in order to include realistic three-dimensional nonlinear responses and the participating mass of the corresponding concrete abutment and mobilized embankment soil. The interaction between the soil and the abutments was reproduced with the two springs (embankment non-linear springs, Figure 2) that were modelled in OpenSees with the uniaxial material EPP [23], as described below.

The longitudinal response is controlled by elastomeric bearing pads, gap, abutment back wall, abutment piles, and soil backfill material. In particular, prior to impact (or gap closure), the elastomeric bearing pads transmit the seismic forces to the stem wall, piles and backfill soil. After gap closure, the bridge deck transfers the seismic forces to the abutment back walls that mobilize the full passive backfill pressure. In Figure 2, the longitudinal response of the longitudinal elastomeric bearing pads and the gap closure behaviour are illustrated by L1.

The bearing pads were modelled with nonlinear springs (total 3), that represented the stiffness of the bearings in the longitudinal, transversal and vertical directions. Their number and distribution were based on the number and location of the girders in the box, as specified in Table 2. The yield and ultimate displacement of the bearings were set as 150% and 300% of the shear strain, respectively. In order to guarantee that shear failure occurred prior to the sliding of the bearing pad, a dynamic coefficient of friction of 0.40 for neoprene on concrete was used. The two zero-length elements at the extreme locations of

rigid element 2 model the longitudinal backfill backwall and the pile system response of the abutment. The abutment stiffness ( $K_{abut}$ ) and ultimate strength ( $F_{abut}$ ) were obtained from Caltrans [30,31], as specified below.

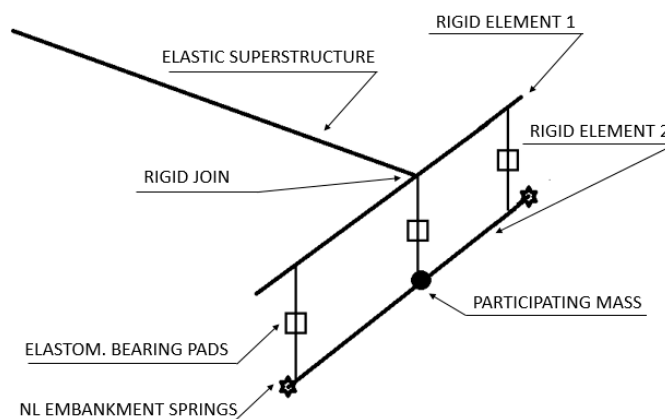


Figure 2. Abutment model: general scheme.

The transverse response was determined by the stiffness of the elastomeric bearing pads and the shear keys; their strength assumed as 30% of the superstructure dead load. In this regard, a hysteretic material was considered by defining a tri-linear response backbone curve with two hardening and one softening stiffness values (more details in [29]). The transversal behaviour was modelled with distributed zero-length elements along two rigid elements to represent the combined behaviour due to the superstructure rotation about the vertical bridge axis (Figure 2). It is worth noting that the bearing pads created a series system between the two transverse rigid elements (rigid element 1 and 2). Rigid element 1 was connected to the deck end by a rigid joint. Figure 2 shows the parallel system of transverse bearing pads and shear keys with T1. In order to compute the transverse stiffness and strength of the backfill, the wing wall and the pile system were defined by considering a series of elements: (1) a rigid one with shear and moment releases, (2) a gap with boundary conditions at each end (that allows only transversal translation), and (3) a zero-length with an elastic-perfectly-plastic (EPP) backbone curve with abutment stiffness ( $K_{abut}$ ) and ultimate strength ( $F_{abut}$ ), obtained from [31]. The stiffness and strength were distributed equally to the two extreme zero-length elements (T2) of rigid element 2.

The vertical response of the abutment was modelled with: (1) the vertical stiffness of the bearing pads (V1), and (2) the vertical stiffness of the trapezoidal embankment (V2). In order to obtain a lumped value, the critical length was introduced inside the formulation proposed by [31,32] to calculate the stiffness per unit length of embankment. The nominal mass of the abutment was assumed proportional to the superstructure dead load (including the structural concrete and the soil mass). The participating mass of the embankment was calculated by considering an average of the embankment lengths obtained from [31].

In order to consider representative cases where the seismic response of the bridge is dominated by the abutments, the criterion (6.3.1.3-1) from [30] was considered, and the abutment displacement coefficient,  $R_A$  was calculated as:

$$R_A = \frac{\Delta_D}{\Delta_{eff}} \quad (1)$$

where  $\Delta_D$  is the longitudinal displacement demand at the abutment and for single-span bridges, which needs to be determined by following point 4.2.1 from [30]:

- (1) the tributary weight of the superstructure and the effective abutment longitudinal stiffness were calculated to determine the structure period,  $T$ , using Equation C4.2.1-1 from [30]:

$$T = 2\pi \sqrt{\frac{W}{g \times K}} \tag{2}$$

where  $g$  is the acceleration due to gravity;

- (2) The spectral acceleration ( $Sa$ ), by introducing the period inside the design spectrum that was chosen as the maximum between the selected ones (SCS: PGA: 0612g; PGV: 116.85 cm/s and PGD: 54.19 cm, see Figure 3); and

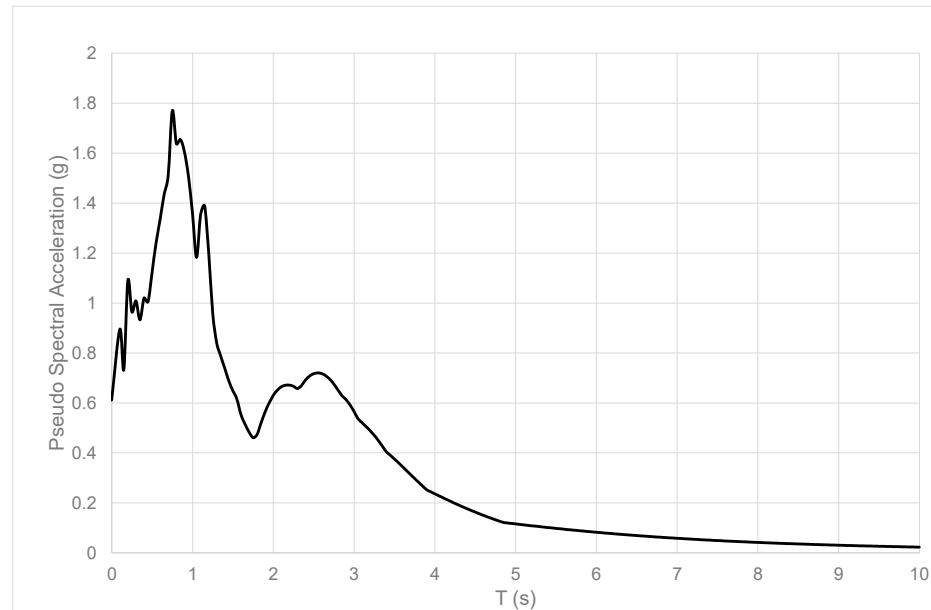


Figure 3. SCS spectrum used as design spectrum for calculation of  $Sa$ .

- (3) The longitudinal displacement demand ( $\Delta_D$ ), which was determined from Equation 4.2.1-1 from [30]:

$$\Delta_D = \frac{W \times Sa}{K} \tag{3}$$

Table 3 shows the calculation of the longitudinal displacement demand at the abutment ( $\Delta_D$ ), by assuming the design spectra for the three considered single-span bridges.

Table 3. Calculation of longitudinal displacement demand ( $\Delta_D$ ).

	W (kN)	T (s)	K (kN/m)	Sa	$\Delta_D$ (m)
B1	935	0.185	11,500	1.01	0.0086
B2	1440	0.245	96,450	0.97	0.0144
B3	2000	0.360	62,300	0.93	0.0230

$\Delta_{eff}$  is the effective abutment longitudinal displacement when the passive force reaches  $F_{abut}$  (in).

$F_{abut}$  (in) was defined by [30] (6.3.1 2-4) and (6.3.1 2-5), respectively, as:

$$F_{abut} = w_{abut} \left( \frac{5.5h_{abut}^{2.5}}{1 + 2.37h_{abut}} \right) R_{sk} \tag{4}$$

$$k_{abut} = w_{abut}(5.5h_{abut} + 20)R_{sk} \tag{5}$$

where:

$h_{abut}$  needs to be taken as  $h_{bw}$  for seat abutments,  
 $w_{abut}$  needs to be taken as  $w_{bw}$  for seat abutments, and  
 $R_{sk}$  is taken as 1 for non-skew bridges.

In addition, following [30] (C6.3.1.1), bilinear representation of the full nonlinear abutment backbone curve was considered. Therefore, for seat-type abutments,  $\Delta_{eff}$  corresponds to the sum of the width of the expansion gap at the seat abutment ( $\Delta_{gap}$ ) and abutment displacement at idealized yield ( $\Delta_{abut}$ ), formula 6.3.1.2-2, by [30].  $\Delta_{abut}$  is calculated as the ratio between the idealized ultimate passive capacity of the backfill behind the abutment backwall ( $F_{abut}$ ) and the abutment longitudinal stiffness ( $K_{abut}$ ).

Table 4 shows the calculation of the effective abutment longitudinal displacement ( $\Delta_{eff}$ ) and the abutment displacement coefficient (RA) for the three considered single-span bridges. It can be observed that RA was less than 2 for all the three configurations, demonstrating that the bridge response was dominated by the abutments.

**Table 4.** Calculation of the effective longitudinal displacement ( $\Delta_{eff}$ ).

	h (ft)	w (ft)	Fbw	kabut	$\Delta_{abut}$ (m)	$\Delta_{gap}$ (m)	$\Delta_{eff}$ (m)	RA
B1	1.3	92	239	2498	0.096	0.0254	0.121	0.07
B2	1.4	95	281	2632	0.106	0.0254	0.132	0.109
B3	1.5	100	333	2825	0.118	0.0254	0.143	0.209

Overall, it is important to consider that the presented model was created according to the current design procedure [30], under the assumption that the abutment backwall is intended to break off and mobilize the longitudinal resistance of the approach fill. It is considered that the passive earth resistance is activated behind the abutments, so as to protect the foundation from excessive deformations. This approach generally overestimates the stiffness of the entire system, due to the fact that: (1) it does not depend on the 3D geometry of the abutment, and (2) it neglects the contribution of the abutment foundation stiffness.

### 3. Methodology

This section describes the main features of the applied methodology based on performing non-linear analyses and developing analytical fragility curves.

#### 3.1. Seismic Scenario

The seismic scenario was described by 100 input motions, selected from the PEER NGA database (<http://peer.berkeley.edu/nga/> (accessed on 24 May 2022)) that were applied at the base of the models, along the  $x$ -axis (longitudinal direction). This ensemble was selected by verifying that the frequencies of the input motions were close to the fundamental periods of the bridges. The input motions were selected through earlier efforts [33,34], to be representative of seismicity in typical regions of California, and have already been applied in [17,35]. The principal aim was to consider a wide potential scenario with multiple levels of intensities, and, thus, to obtain distributed outputs and develop representative fragility curves. The motions were divided into 5 bins of 20 motions each:

- (1) Moment magnitude ( $M_w$ ) 6.5–7.2 and closest distance (R) 15–30 km;
- (2)  $M_w$  6.5–7.2 and R 30–60 km;
- (3)  $M_w$  5.8–6.5 and R 15–30 km;
- (4)  $M_w$  5.8–6.5 and R 30–60 km; and
- (5)  $M_w$  5.8–7.2 and R 0–15 km.

The cumulative density function (CDF) of the selected motions is shown in Figure 4, where the peak ground acceleration (PGA) is the reference intensity measure.

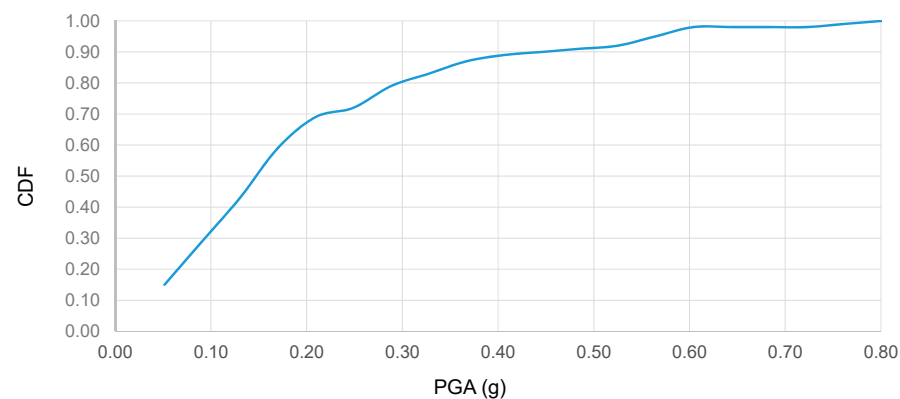


**Figure 4.** Cumulative distributions for PGA.

### 3.2. Fragility Curves

This probabilistic-based approach consists of expressing the relationship between the likelihood of exceeding threshold limits of damage for certain levels of demand (as described in [36]). The damage of the abutments was defined by considering the longitudinal displacement between the deck and the abutments and referring to two limit states: 102 mm and 305 mm as slight (SL1) and moderate (SL2) damage states, respectively. The results of the analyses were calculated for the three models (B1, B2 and B3) for the 100 selected input motions, by considering several intensity measures ( $I_m$ ). In particular, the present study assumed that the uncertainties may be represented by lognormal distributions and, thus, the logarithmic mean ( $\mu$ ) and standard deviation ( $\beta$ ) of the lognormal seismic intensity measure were considered in the development of fragility curves. The responses of the ( $100 \times 3 = 300$ ) analyses were considered to build linear regressions, necessary to calculate the values of the mean and the log-standard deviation. The probability of exceedance ( $PE$ ) was then calculated as:

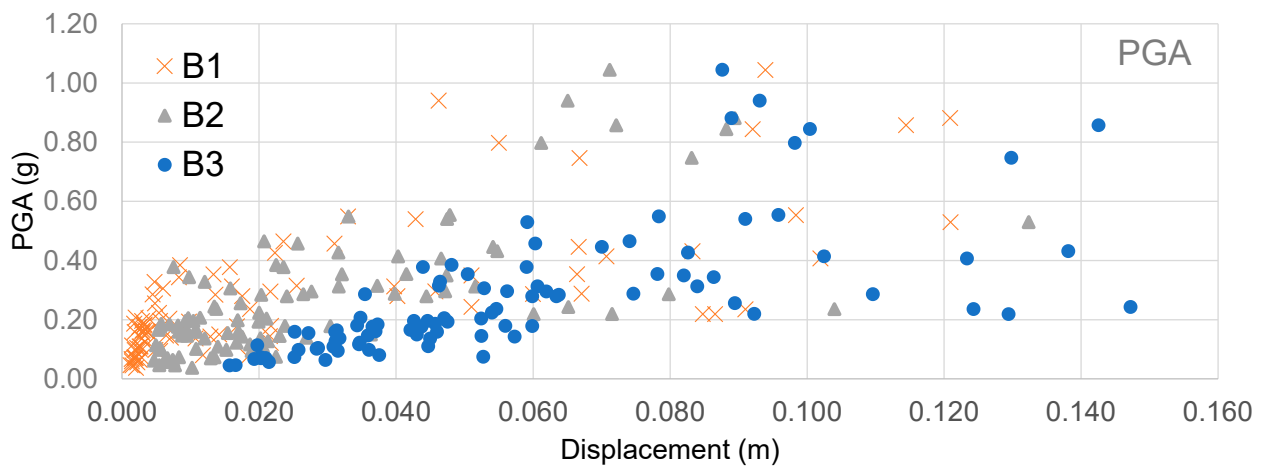
$$PE[D \geq C_i | I_m] = \phi\left(\frac{\ln(I_m) - \mu}{\beta}\right) \quad (6)$$

where:

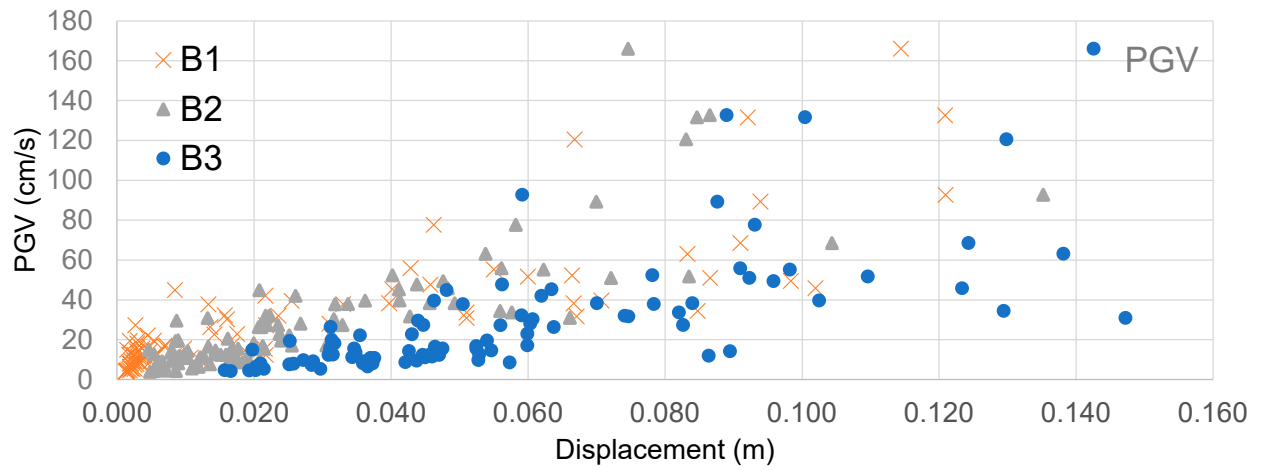
$PE$  is the probability of the structural damage ( $D$ ) to exceed the  $i$ -th damage state ( $C$ ),  
 $\phi$  is the standard normal cumulative distribution function.

## 4. Results

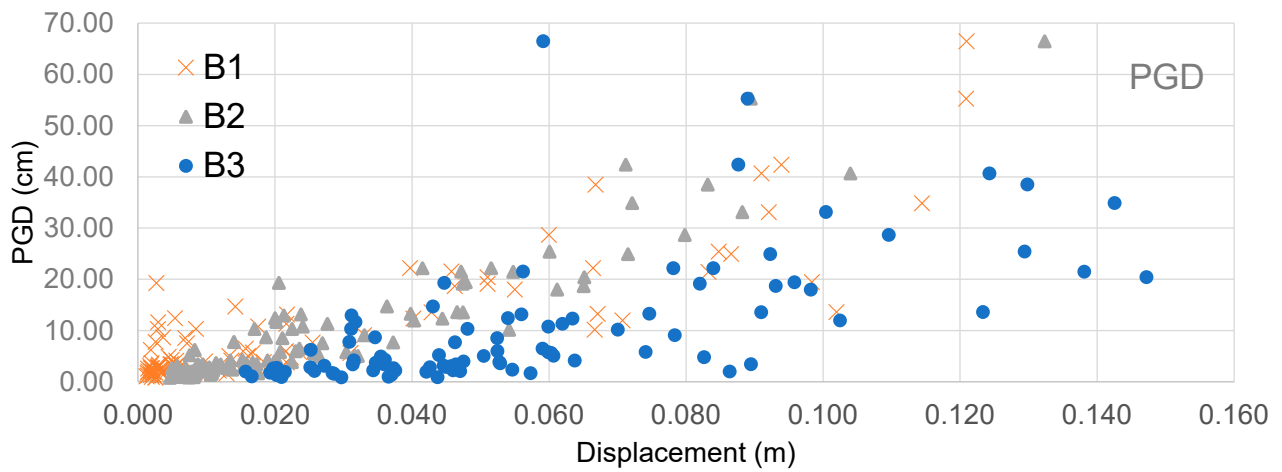
This section describes the results in terms of various intensity measures (peak ground acceleration (PGA) in Figure 5a, peak ground velocity (PGV) in Figure 5b, peak ground displacement (PGD) in Figure 5c, spectral acceleration (SA) in Figure 5d, cumulative absolute velocity (CAV) in Figure 5e, and arias intensity (AI) in Figure 5f), discussing those most suitable to represent the damage at the abutment (longitudinal displacement) and, thus, to develop analytical fragility curves. In particular, Table 5 shows the values of the coefficient of determination  $R^2$  that represents the proportion of variance in the displacements that can be explained by the various intensities measures, or the quality of the regression to fit the obtained results for the various models (B1, B2 and B3).



(a)

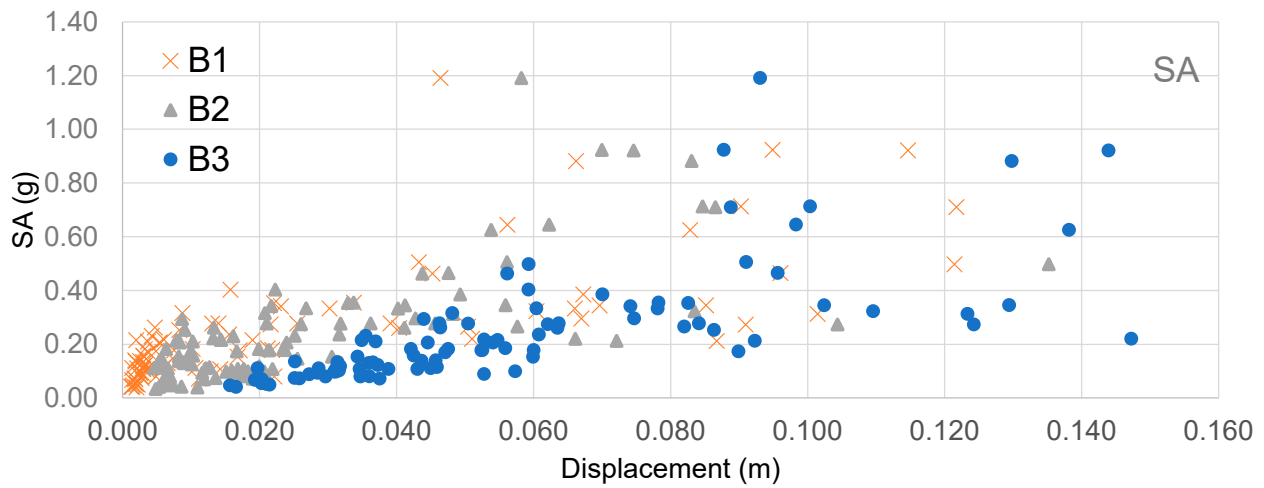


(b)

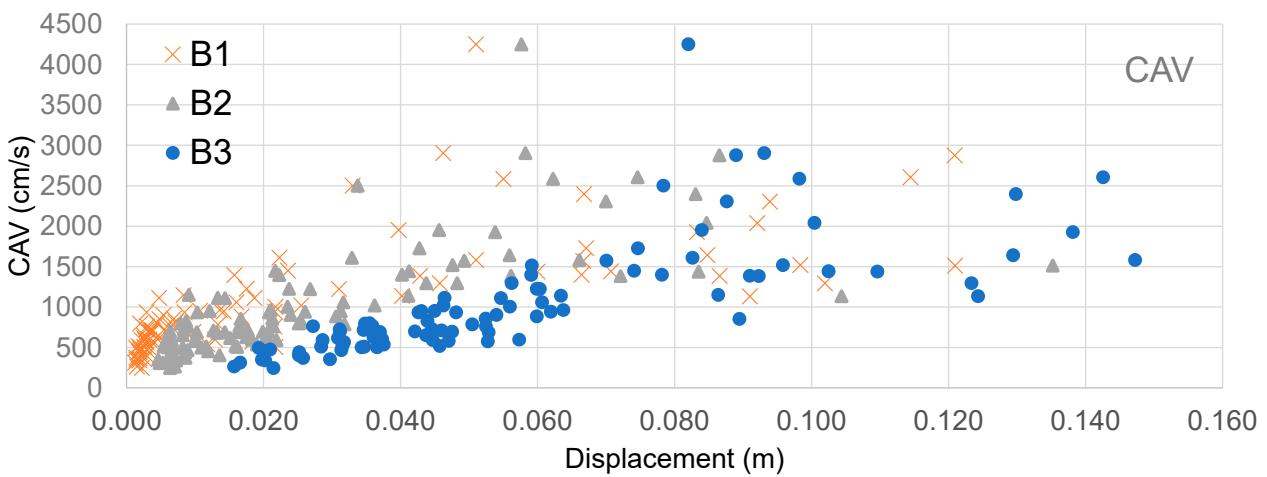


(c)

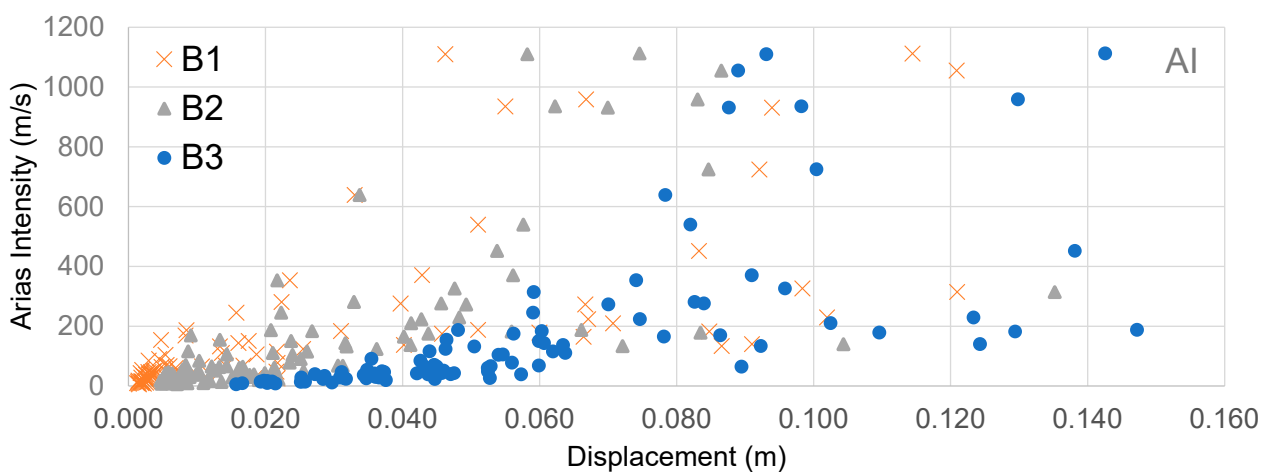
Figure 5. Cont.



(d)



(e)



(f)

**Figure 5.** (a) Displacements vs. PGA for B1, B2 and B3. (b) Displacements vs. PGV for B1, B2 and B3. (c) Displacements vs. PGD for B1, B2 and B3. (d) Displacements vs. SA for B1, B2 and B3. (e) Displacements vs. CAV for B1, B2 and B3. (f) Displacements vs. AI for B1, B2 and B3.

**Table 5.** R<sup>2</sup> for the selected intensity measures (B1, B2 and B3).

R <sup>2</sup>	PGA	PGV	PGD	SA	CAV	AI
B1	0.5204	0.7022	0.7349	0.5261	0.5164	0.4783
B2	0.4903	0.7007	0.8646	0.5002	0.5050	0.4526
B3	0.4486	0.6927	0.8025	0.4887	0.5383	0.4321

### 5. Analytical Fragility Curves

Analytical fragility curves were developed from the above results by considering the peak ground displacement as the intensity measure. Figures 6–8 represent the fragility curves for B1, B2 and B3 for the two selected LSs. It is worth noting that the three models had similar differences among the limit states for all the intensities, meaning that the damage increased with relatively similar trends for the three considered models. For example, at PGD = 10 cm/s, the probability of exceedance (PE) for LS2 was 82.1%, 83.5% and 87.9% more than LS1, for B1, B2 and B3, respectively. B2 and B3 were particularly vulnerable, and LS1 reached values of PE close to 100% for relatively small values of PGD (less than 10 cm/s). In the case of LS2, for high seismicity (more than 30 cm/s), PE reached 100%, demonstrating that the abutments were particularly vulnerable even at relatively small intensities.

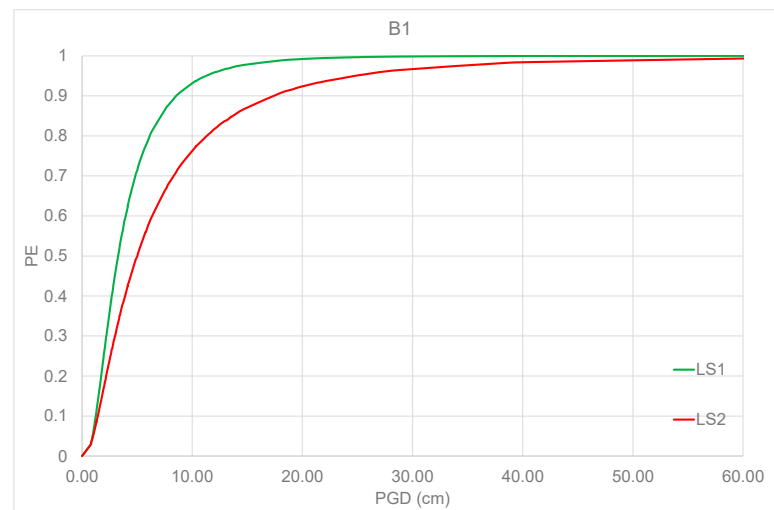


**Figure 6.** B1: relationship between PGD (cm) and the probability of exceedance (PE).

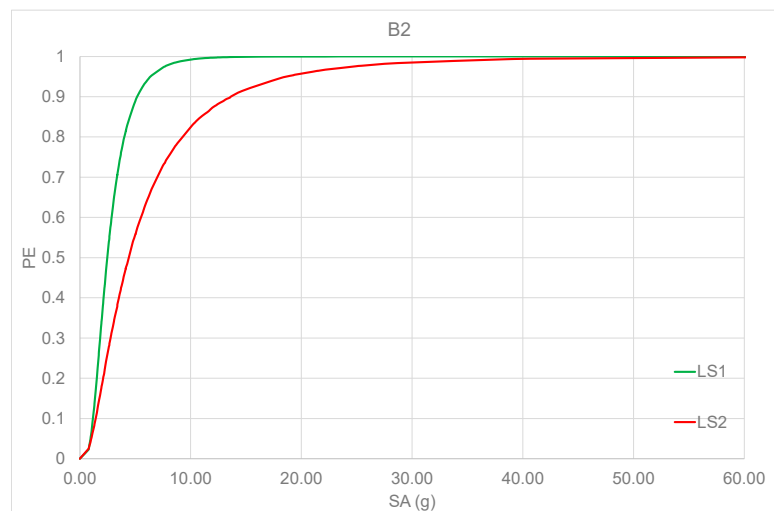


**Figure 7.** B2: relationship between SA (g) and the probability of exceedance (PE).

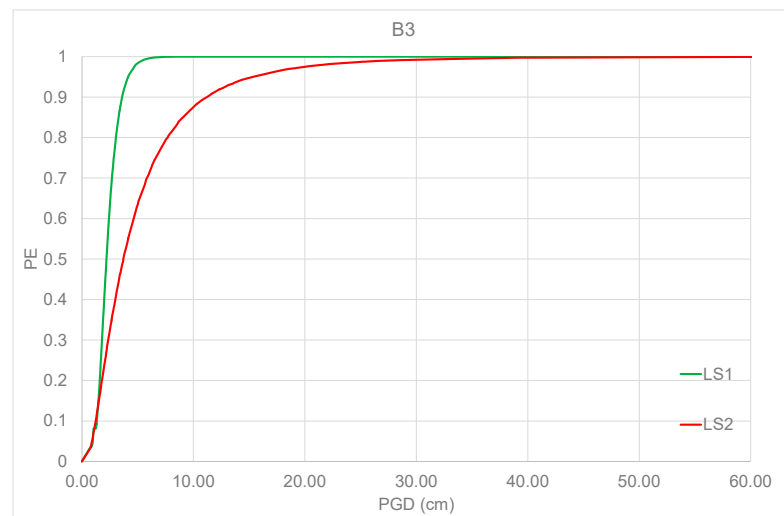


**Figure 8.** B3: relationship between PGD (cm) and the probability of exceedance (PE).

Figures 9 and 10 compare the various configurations for the two considered limit states. It is worth noting from Figure 9 that for PGD = 10 cm/s, PE for model was 93.45% and 99.30% more for model B1 and B2, than the corresponding PE of model B3. Figure 10 maps the derived fragility curves for the most severe damage state (LS2) that was considered in this study. In the case of LS2, the PE values (at PGD = 10 cm/s) for B1 and B2 models were 87.30% and 94.30% more than the corresponding PE of model B3 (more details in Table 6). It is worth noting that the length of the bridge drove its vulnerability, since the more deformable the system became, the more PE increased, shifting the fragility curves toward vulnerable configurations (top left corner). In particular, several outcomes can be deduced:

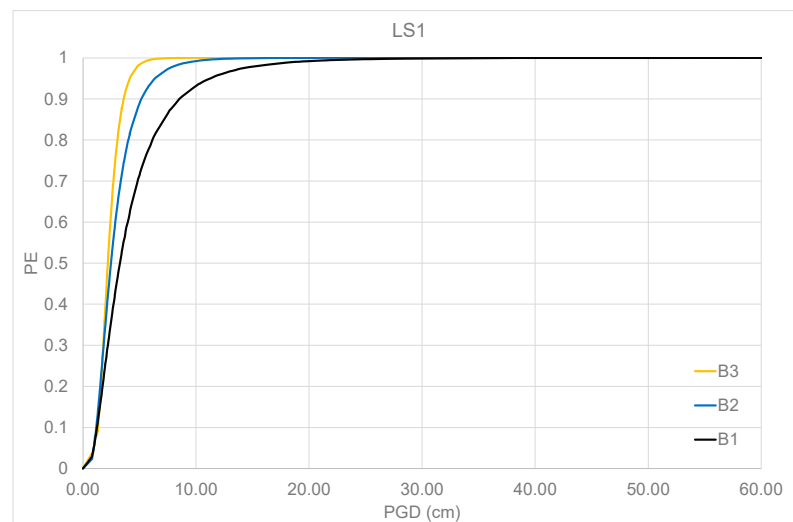


**Figure 9.** Comparison between the models (LS1).

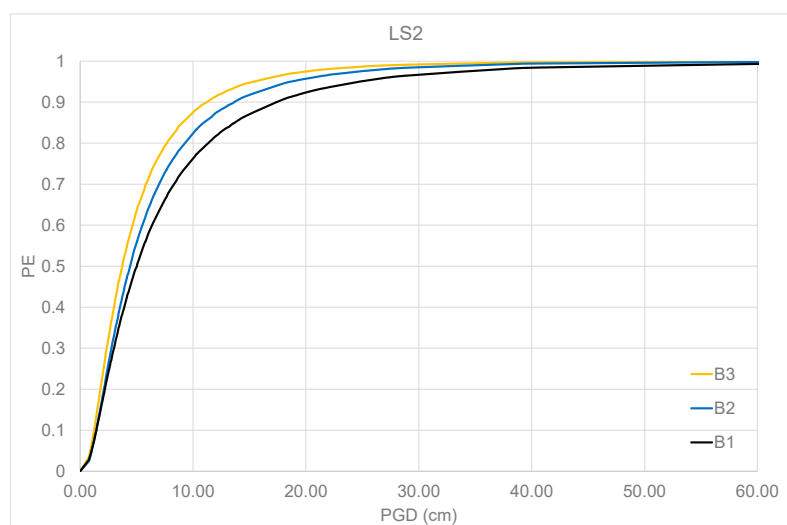


**Figure 10.** Comparison between the models (LS2).

**Table 6.** Comparison of models B1, B2 and B3: PE for LS1 and LS2.

	LS1	Ratio (%)	LS2	Ratio (%)
B1	0.935	93.45	0.767	87.30
B2	0.993	99.30	0.829	94.30
B3	0.999	100	0.879	100

(1) Strengthening the abutments had beneficial effects in reducing the vulnerability of the system to all levels of damage. In particular, this may lead to important design considerations in terms of increasing the stiffness of the abutment bearings by choosing the most suitable system. In this regard, the presented methodology gives an easy-to-read outcome for designers and different stockholders;

(2) This effectiveness was verified for all the considered levels of damage, with a relatively uniform trend, since the performance of the entire bridge depends upon the choice of the bearings. Therefore, it is fundamental to consider that the mechanisms of the bearings may strongly affect the whole bridge behaviour, and bearing design needs to be significantly taken into consideration;

(3) There is a level of PGD after which the shear strains imposed during the seismic excitation reached values that were comparable with bridge deformability. The less deformable the abutments were, the better the entire system behaved. This was another significant finding that needs to be considered in order to calibrate the most performant dynamic characteristics of the bearings, that have been demonstrated to be the core of the design.

Overall, these results demonstrate that the seismic response of the bridge is dominated by the abutments, since the three models were selected by following Caltrans specifications (criterion 6.3.1.3-1 from [30]). In addition, at relatively small intensities, the abutments began to perform non-linear responses that were possible to be investigated by OpenSees. The presented results are limited to the selected case studies and future studies are necessary to propose design considerations and code provisions.

## 6. Conclusions

This paper developed fragility curves for three single-span bridge configurations with the aim of studying the role of abutments in the seismic vulnerability of the structure. The configurations were selected on the basis of Caltrans specifications (criterion 6.3.1.3-1) to ensure that the responses were dominated by the abutments. The performance was studied by considering the damage at the abutment in terms of longitudinal displacements. The

paper investigated the most suitable intensity measure that may realistically represent the damage at the abutments under the selected conditions. The non-linear numerical models performed by OpenSees were fundamental to realistically assess the complexity of the bridge–abutment mechanisms. The developed fragility curves showed that the seismic behaviour of the system depends on the deformability of the bridge, mainly the length. These outcomes may be considered in future proposals of code provisions that account the role of abutments on the seismic vulnerability of single-span bridges.

**Funding:** This research received no external funding.

**Institutional Review Board Statement:** Not applicable.

**Informed Consent Statement:** Not applicable.

**Data Availability Statement:** Not applicable.

**Conflicts of Interest:** The authors declare no conflict of interest.

## References

1. Gehl, P.; Seyedi, D.M.; Douglas, J. Vector-valued fragility functions for seismic risk evaluation. *Bull. Earthq. Eng.* **2013**, *11*, 365–384. [[CrossRef](#)]
2. Sousa, L.; Silva, V.; Marques, M.; Crowley, H.; Pinho, R. Including multiple IMTs in the development of fragility functions for earthquake loss estimation. In Proceedings of the Vulnerability, Uncertainty, and Risk: Quantification, Mitigation, and Management, CDRM 9—American Society of Civil Engineers, Liverpool, UK, 13–16 July 2014; pp. 1716–1725.
3. Padgett, J.E.; Nielson, B.G.; DesRoches, R. Selection of optimal intensity measures in probabilistic seismic demand models of highway bridge portfolios. *Earthq. Eng. Struct. Dyn.* **2008**, *37*, 711–726. [[CrossRef](#)]
4. Zelaschi, C.; Monteiro, R.; Pinho, R. Critical assessment of intensity measures for seismic response of Italian RC bridge portfolios. *J. Earthq. Eng.* **2017**, *23*, 1342293. [[CrossRef](#)]
5. HAZUS. *Multi-Hazard Loss Estimation Methodology Earthquake Model*; Federal Emergency Management Agency: Washington, DC, USA, 2003.
6. Kohrangi, M.; Bento, R.; Lopes, M. Seismic performance of irregular bridges—comparison of different nonlinear static procedures. *Struct. Infrastruct. Eng.* **2015**, *11*, 1632–1650. [[CrossRef](#)]
7. Pinho, R.; Marques, M.; Monteiro, R.; Casarotti, C.; Delgado, R. Evaluation of nonlinear static procedures in the assessment of building frames. *Earthq. Spectra* **2013**, *29*, 1459–1476. [[CrossRef](#)]
8. Pinho, R.; Monteiro, R.; Casarotti, C.; Delgado, R. Assessment of continuous span bridges through nonlinear static procedures. *Earthq. Spectra* **2009**, *25*, 143–159. [[CrossRef](#)]
9. Ebrahimian, H.; Jalayer, F.; Lucchini, A.; Mollaioli, F.; Manfredi, G. Preliminary ranking of alternative scalar and vector intensity measures of ground shaking. *Bull. Earthq. Eng.* **2015**, *13*, 2805–2840. [[CrossRef](#)]
10. Giovenale, P.; Cornell, C.A.; Esteva, L. Comparing the adequacy of alternative ground motion intensity measures for the estimation of structural responses. *Earthq. Eng. Struct. Dyn.* **2004**, *33*, 951–979. [[CrossRef](#)]
11. Bianchini, M.; Diotallevi, P.; Baker, J.W. Prediction of inelastic structural response using an average of spectral accelerations. In Proceedings of the 10th International Conference on Structural Safety and Reliability (ICOSSAR09), Osaka, Japan, 13–17 September 2009; p. 1317.
12. Eads, L.; Miranda, E.; Lignos, D.G. Average spectral acceleration as an intensity measure for collapse risk assessment. *Earthq. Eng. Struct. Dynam.* **2015**, *44*, 2057–2073. [[CrossRef](#)]
13. Biasio, M.D.; Grange, S.; Dufour, F.; Allain, F.; Petre-Lazar, I. A simple and efficient intensity measure to account for nonlinear structural behavior. *Earthq. Spectra* **2014**, *30*, 1403–1426. [[CrossRef](#)]
14. Baker, J.W. Efficient analytical fragility function fitting using dynamic structural analysis. *Earthq. Spectra* **2015**, *31*, 579–599. [[CrossRef](#)]
15. Baker, J.W.; Cornell, C.A. Vector-valued intensity measures incorporating spectral shape for prediction of structural response. *J. Earthq. Eng.* **2008**, *12*, 534–554. [[CrossRef](#)]
16. Bayat, M.; Daneshjoo, F.; Nistico, N. A novel proficient and sufficient intensity measure for probabilistic analysis of skewed highway bridges. *Struct. Eng. Mech.* **2015**, *55*, 1177–1202. [[CrossRef](#)]
17. Forcellini, D.; Alzabeebee, S. Seismic fragility assessment of geotechnical seismic isolation (GSI) for bridge configuration. *Bull. Earthq. Eng.* **2021**. [[CrossRef](#)]
18. Mackie, K.R.; Stojadinović, B. Performance-based seismic bridge design for damage and loss limit states. *Earthq. Eng. Struct. Dyn.* **2007**, *36*, 1953–1971. [[CrossRef](#)]
19. Zentner, I. A general framework for the estimation of analytical fragility functions based on multivariate probability distributions. *Struct. Saf.* **2017**, *64*, 54–61. [[CrossRef](#)]

20. Romstad, K.; Kutter, B.; Maroney, B.; Vanderbilt, E.; Griggs, M.; Chai, Y.H. *Experimental Measurements of Bridge Abutment Behavior*; Rep. No. UCD-STR-95-1; Department of Civil and Environmental Engineering, University of California: Davis, CA, USA, 1995.
21. Bozorgzadeh, A. Effect of Backfill on Stiffness and Capacity of Bridge Abutments. Ph.D. Thesis, University of California, San Diego, CA, USA, 2007.
22. Lemnitzer, A.; Ahlberg, E.; Nigbor, R.; Shamsabadi, A.; Wallace, J.; Stewart, J. Lateral Performance of Full-Scale Bridge Abutment Wall with Granular Backfill. *J. Geotech. Geoenviron. Eng.* **2009**, *135*, 506–514. [[CrossRef](#)]
23. Mazzoni, S.; McKenna, F.; Scott, M.H.; Fenves, G.L. *Open System for Earthquake Engineering Simulation, User Command-Language Manual*; 2009; Available online: <http://opensees.berkeley.edu/OpenSees/manuals/usermanual> (accessed on 24 May 2022).
24. Mina, D.; Forcellini, D. Soil–Structure Interaction Assessment of the 23 November 1980 Irpinia-Basilicata Earthquake. *Geosciences* **2020**, *10*, 152. [[CrossRef](#)]
25. Forcellini, D. 3D Numerical simulations of elastomeric bearings for bridges. *Innov. Infrastruct. Solut.* **2016**, *1*, 1–9. [[CrossRef](#)]
26. Forcellini, D. Assessment on geotechnical seismic isolation (GSI) on bridge configurations. *Innov. Infrastruct. Solut.* **2017**, *2*, 1–6. [[CrossRef](#)]
27. Lam, I.; Martin, G.R. *Seismic Design of Highway Bridge Foundations*; U.S. Department of Transportation, Federal Highway Administration, Research, Development, and Technology: Washington, DC, USA, 1986.
28. Aviram, A.; Mackie, K.R.; Stojadinovic, B. Effect of abutment modeling on the seismic response of bridge structures. *Earthq. Eng. Eng. Vib.* **2008**, *7*, 395–402. [[CrossRef](#)]
29. Kotsoglu, A.; Pantazopoulou, S. Modeling of Embankment Flexibility and Soil-structure Interaction in Integral Bridges. In Proceedings of the First European Conference on Earthquake Engineering and Seismology, Geneva, Switzerland, 3–8 September 2006.
30. Caltrans. *Caltrans Seismic Design Criteria*; Version 2.0; California Department of Transportation; Sacramento, CA, USA, 2019.
31. Zhang, J.; Makris, N. Kinematic Response Functions and Dynamic Stiffnesses of Bridge Embankments. *Earthq. Eng. Struct. Dyn.* **2002**, *31*, 1933–1966. [[CrossRef](#)]
32. Werner, S.D. Study of Caltrans’ Seismic Evaluation Procedures for Short Bridges. In Proceedings of the 3rd Annual Seismic Research Workshop, Sacramento, CA, USA, 27–29 June 1994.
33. Gupta, A.; Krawinkler, H. Estimation of seismic drift demands for frame structures. *Earthq. Eng. Struct. Dyn.* **2000**, *29*, 1287–1305. [[CrossRef](#)]
34. Mackie, K.R.; Wong, J.-M.; Stojadinovic, B. *Integrated Probabilistic Performance-Based Evaluation of Benchmark Reinforced Concrete Bridges*; Report No. 2007/09; Pacific Earthquake Engineering Research Center, University of California: Berkeley, CA, USA, 2007.
35. Forcellini, D. Cost assessment of isolation technique applied to a benchmark bridge with soil structure interaction. *Bull. Earthq. Eng.* **2017**, *15*, 51–69. [[CrossRef](#)]
36. Mina, D.; Forcellini, D.; Karampour, H. Analytical fragility curves for assessment of the seismic vulnerability of HP/HT unburied subsea pipelines. *Soil Dyn. Earthq. Eng.* **2020**, *137*, 106308. [[CrossRef](#)]